The Cryosphere Discuss., https://doi.org/10.5194/tc-2019-91
Manuscript under review for journal The Cryosphere
Discussion started: 15 May 2019


# Estimation of soil properties by coupled inversion of electrical resistance, temperature, and moisture content data

Elchin E. Jafarov[1], Dylan R. Harp[1], Ethan T. Coon[2], Baptiste Dafflon[3], Anh Phuong Tran[3,4], Adam L. Atchley[1], Cathy J. Wilson[1], and Youzuo Lin[1]

1. Earth and Environmental Sciences Division, Los Alamos National Laboratory, Los Alamos, New Mexico, USA
2. Climate Change Science Institute and Environmental Sciences, Oak Ridge National Laboratory, Oak Ridge, Tennessee, USA
3. Climate and Ecosystem Division, Lawrence Berkeley National Laboratory, Berkeley, California, USA
4. Department of Water Research Engineering and Technology, Water Research Institute, Hanoi, Vietnam

## Abstract

Studies indicate greenhouse gas emissions following permafrost thaw will amplify current rates of atmospheric warming, a process referred to as the permafrost carbon feedback (PCF). However, large uncertainties exist regarding the timing and magnitude of the PCF, in part due to uncertainties associated with subsurface permafrost parameterization and structure. Development of robust parameter estimation methods for permafrost-rich soils is becoming urgent under accelerated warming of the Arctic. Improved parameterization of the subsurface properties in land system models would lead to improved predictions and reduction of modeling uncertainty. In this work we set the groundwork for future parameter estimation (PE) studies by developing and evaluating a joint PE framework that estimates soil properties from time-series of soil temperature, moisture, and electrical resistance measurements. The framework utilizes the PEST (Model Independent Parameter Estimation and Uncertainty Analysis) toolbox and coupled hydro-thermal-geophysical modeling. We test the framework against synthetic data, providing a proof-of-concept for the approach. We use specified subsurface parameters and coupled models to setup a synthetic state,

perturb the parameters, then verify that our PE framework is able to recover the parameters and synthetic state. To evaluate the accuracy and robustness of the approach we perform multiple tests for a perturbed set of initial starting parameter combinations. In addition, we evaluate the relative worth of including various types and amount of data needed to improve predictions. The results of the PE tests suggest that using data from multiple observational datasets improves the accuracy of the estimated parameters.

## 1. Introduction

Subsurface soil property parametrization contributes to a wide uncertainty range in projected active layer depth and in simulated permafrost distribution in the Northern Hemisphere when predicted using Land System Models (LSM) (Koven et al., 2015; Harp et al., 2016). Reduction of this uncertainty is becoming urgent with recent accelerated thawing of permafrost (Biskaborn et al., 2019). Warming permafrost leads to increase infrastructure maintenance costs (Hjort et al., 2018), has a positive feedback on global climate change (McGuire et al., 2018), and increases the probability of the potential hazards for human health (Schuster et al., 2018). Better subsurface soil property parametrizations in LSMs requires the development of methods that can robustly estimate these soil properties including porosity and thermal conductivity of peat and mineral layers.

Direct measurements of subsurface soil properties are labor intensive, destructive, and not always feasible (Smith and Tice, 1988; Kern, 1994; Boike and Roth, 1997; Yoshikawa et al., 2004). While soil sample analysis can provide critical information on soil properties at a fine scale, this information is limited to sparsely sampled locations. Multiple methods used in the laboratory to measure soil properties by using soil cores extracted from the field site are well summarized by Nicolsky et al., (2009), but logistical and economic burden typically do not allow these measurements to be made in the field. Inverse modeling serves as an alternative approach to recover soil properties using a combination of indirect measurements and physics-based numerical models.

Different inverse modeling frameworks have been developed to estimate soil thermal properties using physical-based models and time-series of soil moisture, temperature and/or geophysical data. Many use a heat equation without phase change (Beck et al., 1985; Allifanov et al., 1996). More recent works include phase change, which is an important component of the energy balance in permafrost-affected soils (e.g. Nicolsky et al., 2007; 2009, Tran et al., 2017). Nicolsky et al., (2007; 2009) used an optimization based inverse method and a variational data assimilation method to estimate soil properties. Harp et al., (2016) used an ensemble-based method to evaluate the uncertainty of projections of permafrost conditions in a warming climate due to uncertainty in subsurface properties. Atchley et al., (2015) used data calibration to estimate hydrothermal properties of soils. All these methods used ground temperature timeseries alone to estimate soil properties through their role in modulating heat fluxes. Moreover, all these methods utilized 1D soil columns and therefore assume 1D soil structure.

Recently, Tran et al., (2017) used a coupled hydrological–thermal–geophysical modeling approach to estimate soil organic content. The approach was based on coupling the 1D Community Land Model (CLM4.5; Oleson et al., 2013) that simulates surface-subsurface water, heat and energy exchange and the 2D Boundless Electrical Resistivity Tomography (BERT) forward model (Rücker et al., 2006). The simulated 1D profiles of the subsurface temperature, liquid water content and ice content from CLM model were explicitly linked to soil electrical resistivities via petrophysical relationships and then to soil electrical resistances using the BERT forward model. Here we modify and extend this approach to 2D by using the Advanced Terrestrial Simulator (ATS) model, which was specifically developed to study fine-scale hydrothermal processes of permafrost-affected soils. In addition, instead of estimating organic content of the soil as in Tran et al., (2017), we estimate properties of peat (organic) and mineral layers across a 2D transect within polygonal tundra.

Modeling the full, continuous 2D transect allows us to simulate lateral hydro-thermal fluxes not possible with individual 1D columns known to be important in polygonal tundra (Abolt et al, 2018, Liljedahl et al, 2016). At each grid cell in the transect, a unique state develops during the ATS simulation (temperature, saturation, etc.) that is then used to calculate heterogeneous electrical resistivities via petrophysical relations. This allows more realistic simulated electrical resistances that include the effects of lateral hydrothermal connectivity within the transect.

Through this approach, we develop a parameter estimation (PE) framework that is able to estimate subsurface properties in permafrost-affected soils through joint inversion of hydrothermal and geophysical measurements. Our main objective then is to evaluate which types and number of measurements are necessary to constrain the inversion to yield a robust and accurate prediction of subsurface properties. The method jointly inverts based on matching multiple types of measurements (temperature, saturation, and electrical resistivity) using a forward modeling framework that couples a state-of-the-art hydrothermal permafrost simulator with an electrical resistance simulator. We progressively test the accuracy and robustness of the method using a series of synthetic problems by: 1) increasing the complexity of the meteorological data used to drive the coupled thermo-hydro-geophysical model and 2) testing the inclusion of individual and combinations of several available measurement types on the accuracy and repeatability of inversions. We further used findings from this study to suggest how data should be collected to improve the accuracy of the estimated soil properties and to optimize total number measurements needed to make a robust subsurface PE. The results of this work can be used to better understand uncertainties associated with subsurface soil property estimation. In addition, the approach can be used to inform field campaigns to ensure that sufficient measurements are collected to allow soil property estimation at a desired accuracy.

## 2. Methods

We estimate effective soil properties for peat and mineral layers of a 2D transect within polygonal tundra. Our PE approach is summarized in Figure 1. We utilized the Advanced Terrestrial Simulator model version 0.86 (ATS), a fully 3D-capable coupled groundwater flow and heat transport model representing the soil physics needed to capture permafrost dynamics, including ice, air, and liquid saturation, flow of unfrozen water in the presence of phase change, and non-homogeneous soil layering (Painter et al., 2016). We sequentially coupled ATS with the Boundless Electrical Resistivity Tomography (BERT) model (Rücker et al., 2006), which we run in forward mode to compute ERT survey resistance values based on soil resistivities calculated using ATS output (temperatures, saturations, etc.) and petrophysical relations. The forward mode of BERT solves Poisson's equation using the finite-element method to calculate ERT survey resistances in a two-dimensional tomography corresponding to the cross section of the ice-wedge polygonal tundra site.

The Cryosphere Discuss., https://doi.org/10.5194/tc-2019-91
Manuscript under review for journal The Cryosphere
Discussion started: 15 May 2019


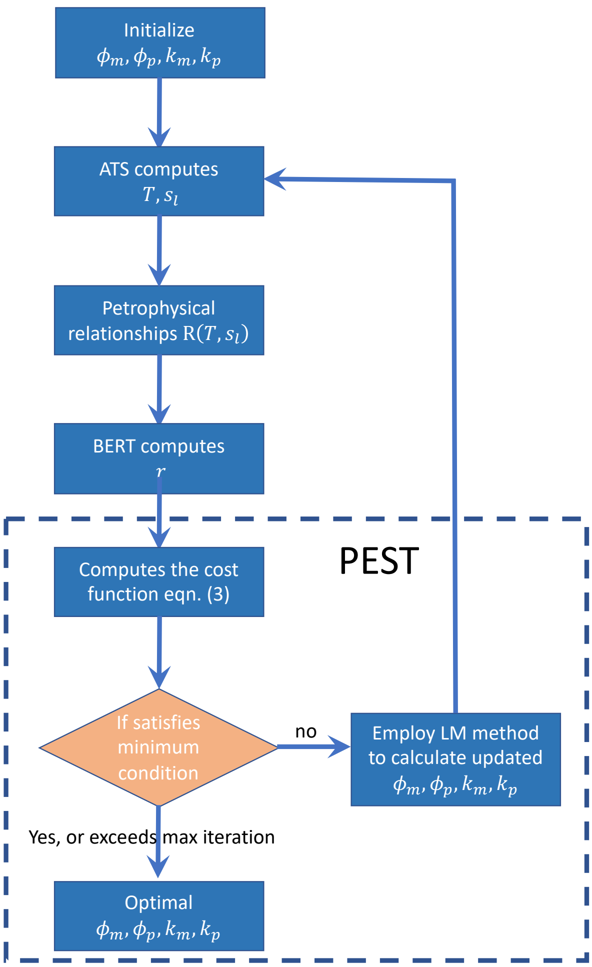


**Figure 1.** Schematics of the parameter estimation algorithm.

### 2.1 Synthetic Model

To setup the synthetic model, we used digital elevation data of a transect through ice-wedge polygonal tundra at the Barrow Environmental Observatory (BEO), at Utqiagvik, Alaska. The mesh shown on Figure 2A represents the cross-section of the polygonal tundra. Thickness of the peat (organic) layer corresponds to observations at the site, with a thick peat layer on the sides (troughs) and thinner in the middle of the low center polygon. A mineral layer was assigned below the peat layer across the transect. We initially designated six synthetic observation (temperature and soil moisture measurement) locations within the active layer thickness (ALT) similar to the sensor setup at the site (Dafflon et al., 2017). Then we added 4 more synthetic observation locations below the ALT (Figure 2B) to better understand the effect of their inclusion on PE accuracy and robustness. All observation locations are represented as stars on Figure 2A corresponding to the locations of the collected temperature and soil moisture timeseries. The temperature and soil moisture timeseries were observed at depth 5, 20, 60, and 80 cm below the surface. The overall depth of the modeling domain is 45 m. We set the bottom boundary to a constant temperature of T=263.55K, and closed (zero heat and mass flux) boundary conditions on the vertical sides. The required steps to establish a water table in permafrost soils in the ATS model have been documented in Atchley et al., (2015) and Jafarov et al., (2018). A seepage face was imposed at 4 cm below the surface on each side of the domain to allow drainage through connected trough networks and preventing water from pooling at the surface, as is typical of partially degraded polygonal ground (Liljedahl et al, 2016). We use two types of meteorological datasets as surface boundary condition drivers for the ATS model: simplified (sinusoidal air temperature, constant precipitation, and constant radiative forcing) and actual weather data from the BEO site. The actual meteorological data were collected starting on January 1, 2015 and includes air temperature, rain and snow precipitation, humidity, long and shortwave radiation and wind speed. We present ground temperatures simulated for the synthetic model run with actual meteorological data in Figure 2B, where the linear white region indicates the ALT within the transect (i.e., 0º C). The deepest ALT is in the middle of the transect (42 cm) and shallowest on the sides (35 cm). In addition, In Figure 3 we present corresponding liquid-water and ice saturation for the synthetic model run at different times of the year.

ATS uses the designated porosities and thermal conductivities $\{\phi, k\}$ of peat and mineral soil layer to compute temperature ($T$) and liquid-water saturation ($s_l$) designated as the synthetic truth. To calculate thermal conductivities of the air-water-ice-soil mixture, the ATS model interpolates between saturated frozen, saturated unfrozen, and fully dry states (Painter et al., 2016) where the thermal conductivities of each end-member state is determined by the thermal conductivity of the components (soil grains, air, water, or liquid) weighted by the relative abundance of each component in the cell (Johansen, 1977; Peters-Lidard et al, 1998; Atchley et al., 2015). Standard empirical fits are used for the internal energy of each component of the air-water-ice-soil mixture. The corresponding equation used to calculate saturated, frozen thermal conductivity ($\kappa_{sat,f}$) has the following form:

$$\kappa_{sat,f} = \kappa_{sat,uf} \cdot \kappa_i^{\phi} \cdot \kappa_w^{-\phi}, \tag{1}$$

The Cryosphere Discuss., https://doi.org/10.5194/tc-2019-91
Manuscript under review for journal The Cryosphere
Discussion started: 15 May 2019


The Cryosphere
Discussions
Open Access

where $\kappa_{sat,uf}$, $\kappa_i$, $\kappa_w$ are thermal conductivities for saturated unfrozen, ice, and liquid water, respectively, and $\phi$ is porosity.

We sequentially couple the ATS and BERT numerical models via petrophysical relationships used by Tran et al., (2017). In that approach, the electrical conductivity is determined as a function of temperature and liquid water saturation:

$$R(T, s_l) = 1/(\phi^d[s_l^n\sigma_w + (\phi^{-d} - 1)\sigma_s] \cdot [1 + c(T - 25)]), \tag{2}$$

where $R(T, s_l)$ is the electrical resistivity, $\sigma_w$ and $\sigma_s$ are the electrical conductivities of water and soil/sediments, respectively, $n$ is a saturation index, $d$ is a cementation index, and $c$ is a temperature compensation factor accounting for deviations from $T = 25^oC$. Calculated electrical resistivities get passed to the BERT model which computes electrical resistances ($r$) such as measured during an ERT survey. In this study we assume all constants used in equation (2) are known (see Tran et al., 2017) and focus on the uncertainty in the simulations instead of the accuracy of parameters used in the petrophysical relationships.

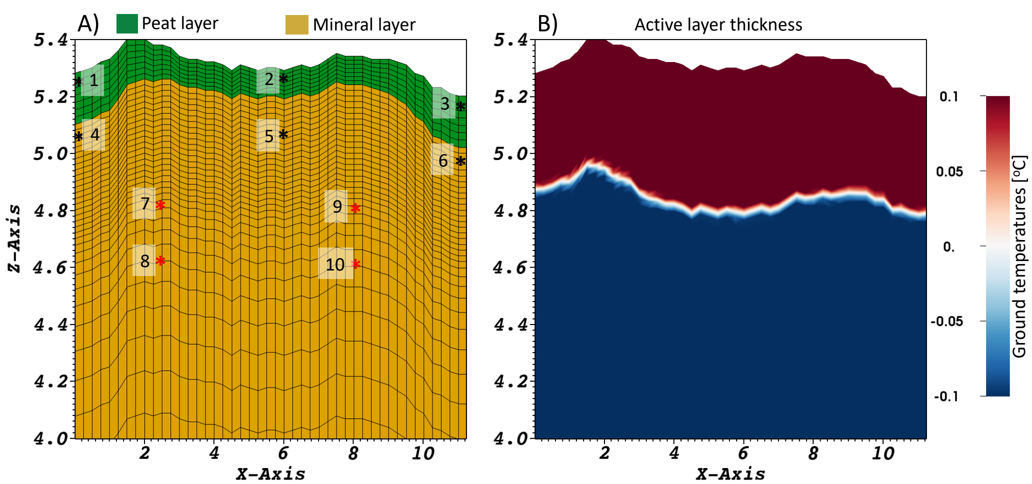


**Figure 2.** A) The (vertically exaggerated for clarity) 2D transect mesh used by the ATS model. Green represents the peat layer and brown represents the mineral soil layer. Black stars correspond to the 6 sensors collecting temperature and soil moisture content within the active layer. Red stars correspond to the 4 sensors collecting temperature and soil moisture content below the active layer. B) Ground temperature distribution simulated by the ATS model, corresponding to the time of maximum subsurface thaw. The active layer thickness corresponds to the linear white region (i.e., 0°C region) dividing the thawed and frozen regions of the ground.

The Cryosphere Discuss., https://doi.org/10.5194/tc-2019-91
Manuscript under review for journal The Cryosphere
Discussion started: 15 May 2019


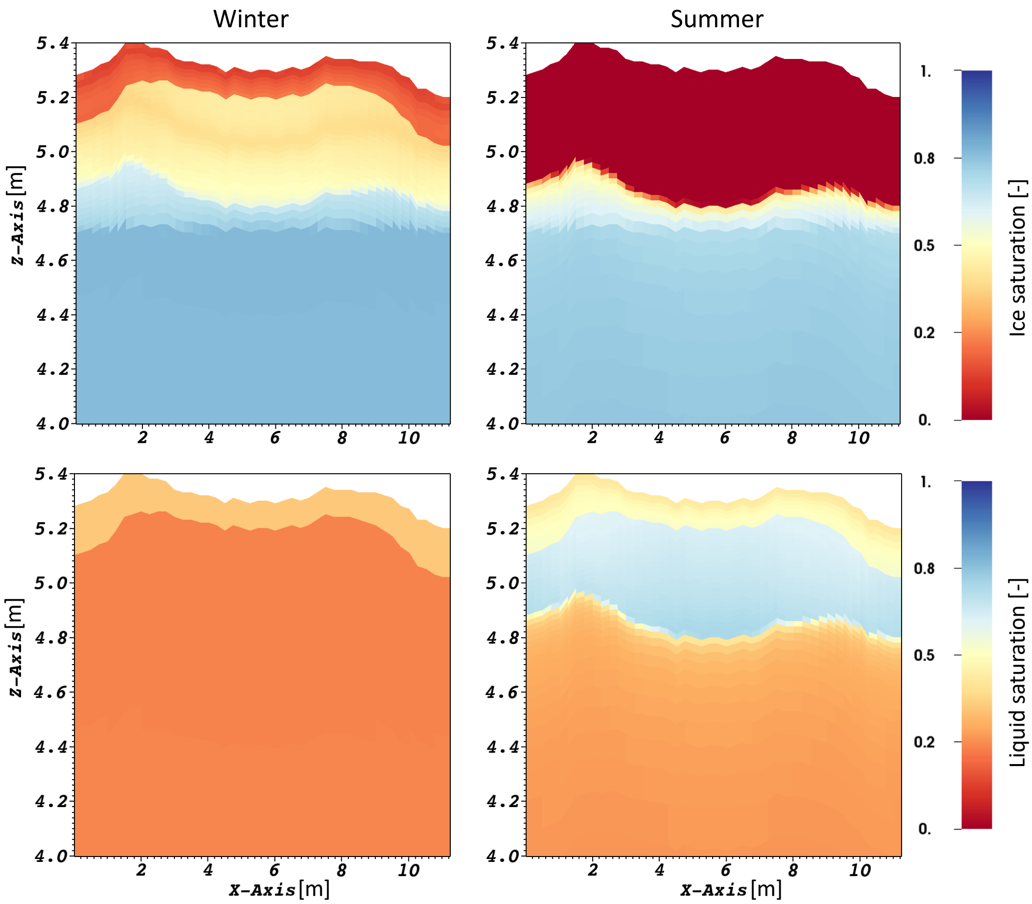


**Figure 3.** Vertical transects of example model simulation results of liquid and ice saturation (rows) over winter and summer time periods (columns).

## 2.2 Parameter estimation

To test if the known soil properties can be recovered, we start with randomly selected initial parameter guesses as if the synthetic truth is unknown. We use a Latin Hypercube Sampling method to generate random initial guesses of porosity and thermal conductivities around the synthetic truth (McKay et al., 1979). Each sample set includes four parameters: porosity and thermal conductivity for peat and mineral soil layers. The rest of the hydrothermal properties are kept fixed. These parameters were chosen due to their strong controls on both hydrologic and thermal states (Atchley et al., 2015, Nicolsky et al., 2009).

The inverse approach involves the minimization of a cost function expressed as the sum-of-squared differences between simulated values and synthetic measurements using the Levenberg-Marquardt (LM) algorithm (K. Levenberg, 1944; D. W. Marquardt 1963) implemented in the PEST software package (Doherty, 2001), which was used to handle all parameter estimation runs.

To estimate soil physical properties, we minimize the cost function ($J$) representing the sum-of-squared differences between the calculated and synthetic $T$, $s_l$, and $r$ in the following form:

$$J(\phi, k) = w_T \sum (T_c - T_s)^2 + w_s \sum \left(s_{l_c} - s_{l_s}\right)^2 + w_r \sum (r_c - r_s)^2, \tag{3}$$

where indices $c$ and $s$ correspond to calculated and synthetic states of the system, $w_T, w_s$, and $w_r$ are the corresponding weights for the temperature, saturation and resistance residuals (differences between calculated and synthetic values).

The weights were chosen in order to scale the contribution of each type of residual so that contributions to the cost function are evenly distributed across temperature, saturation, and resistance residuals. For example, saturation residuals are on the order of a few tenths, while resistance residuals can be tens of ohms. The weights were selected based on evaluating the individual contributions to the cost function for each measurement type on an ensemble of simulations spanning the parameter ranges. The electrical resistance residual weight ($w_r$) was set to one. The temperature and saturation residual weights ($w_T$ and $w_s$) were then modified so that each measurement type component in the cost function had roughly equivalent magnitude over most of the parameter space. This resulted in weights of $w_r$=1, $w_T$=2.5x10$^3$, and $w_s$=3.5x10$^5$.

If the cost function satisfies minimum criteria or the maximum allowed number of iterations, which we chose to be equal to 25, is reached. The subsurface properties corresponding to the minimum of the cost function, i.e., the best fit between simulated and synthetic values, are considered the estimated parameter values as

$$\{\phi, k\} = \underset{\substack{\phi_{min} \le \phi \le \phi_{max}, \\ k_{min} \le k \le k_{max}}}{\operatorname{argmin}} J(\phi, k), \tag{4}$$

here $\{\phi, k\}$ are estimated porosities and thermal conductivities for peat and mineral soil.

Based on sensitivity analyses using simplified meteorological data, the cost function response surface was smooth and convex over the parameter ranges of interest. Therefore, we chose the LM approach because of its robust gradient-based optimization scheme that takes advantage of smooth convex response surfaces to quickly converge to minima.

To build an understanding of the inverse framework, we start with a simple setup and then gradually add more complexity. First, we use simplified meteorological data where we assume that air temperatures change according to a sinusoidal function and all other terms are constants. Initially we started with 3 observational points within the peat layer (refer to Figure 2A) and 1 ERT profile. Then we increase the number of ERT profiles up to 8 by adding profiles once per month from January till August. Each ERT profile calculated by BERT uses the set of daily averaged $T$ and $s_l$ simulated by ATS and petrophysical relations (eqn. 2) which are varying over time. Then we increase the number of observation points to 6 and add noise to the simulated data. Introduction of the noise allows us to evaluate the effect of measurement uncertainties that will be present in the actual application of the PE method. We added different levels of Gaussian noise to the synthetic measurements of $T$, $s_l$, and $r$ in the following way: 1% to $T$, 5% to $s_l$, and 10% to $r$. These levels of noise for the different types of measurements are based on published literature and our own experience (Wang et al., 2018; Dafflon et al., 2017). After that we substitute simplified meteorological data with actual data from the BEO site to evaluate our PE method under realistic ground surface boundary conditions. In this case we evaluate how much and what kind of data do we need to robustly recover subsurface porosities and thermal conductivities. To do this we test the inclusion of individual types of measurements in the cost function (equation 3) as well as all possible combinations of measurement types. We used different soil property ranges for the simplified and actual meteorological data PE runs which are summarized in Table 1. This was done to test the consistency and effectiveness of the PE method. In addition, we compared the difference between estimated parameters for 8 ERT profiles collected once a month for 8 months versus once a day for 8 days. Notation and description of each run for simplified and actual meteorological data is summarized in Table 2.

**Table 1: Allowed range for the estimated subsurface properties.**

| **Properties** | **Simplified meteorological data** | | **Actual meteorological data** | |
|---|---|---|---|---|
| | **peat** | **mineral** | **peat** | **Mineral** |
| Porosity $[m^3 \cdot m^{-3}]$ | 0.8±1.9 | 0.6+0.25 | 0.6±1.9 | 0.4+0.25 |
| Thermal conductivity, $[W\ m^{-1} K^{-1}]$ | 0.225±0.2 | 2.0±0.5 | 0.15±0.1 | 1.6±0.5 |

**Table 2: Description of all PE cases used in this study**.

The Cryosphere Discuss., https://doi.org/10.5194/tc-2019-91
Manuscript under review for journal The Cryosphere
Discussion started: 15 May 2019


| Case number | Simplified meteorological data (S)* | Actual meteorological data |
|---|---|---|
| 1 | (S)$3T3s_l1r$ | $6T$ |
| 2 | (S)$3T3s_l8r$ | $10T$ |
| 3 | (S)$6T6s_l1r$ | $6s_l$ |
| 4 | (S)$6T6s_l8r$ | $1r$ |
| 5 | (S)$6T6s_l1r+n$ | $6T1r$ |
| 6 | (S)$6T6s_l8r+n$ | $6s_l1r$ |
| 7 | | $6T6s_l$ |
| 8 | | $3T3s_l1r$ |
| 9 | | $3T3s_l8r$ |
| 10 | | $6T6s_l8r$ |
| 11 | | $6T6s_l8r(s)$ ** |
| 12 | | $10T10s_l1r$ |
| 13 | | $10T10s_l8r$ |

The numbers before $T$ and $s_l$ correspond to the number of measurement points used. Number before $r$ corresponds to the number of resistance profiles used.

*n* stands for noise added to the synthetic measurements.

*(S) corresponds to runs driven by simplified meteorological data, no (S) corresponds to runs driven with actual meteorological data

**All resistance profiles are taken once per month, except the case with (s) corresponding to sequential daily profiles.

## 3. Results

### 3.1 Simplified meteorological data

To evaluate the PE method performance driven by simplified meteorological data, we ran PE experiments using 30 different random combinations of porosity and thermal conductivity values as the initial starting point. It is important to note that one of the main points of this study is to demonstrate that one or two LM runs might lead to false assumptions about recovered parameters. Multiple runs starting from different initial guess values are necessary to ensure the robust recovery of the subsurface conditions. If most of the LM runs converge to the same set of parameters and have low cost function values, then that set most likely corresponds to the actual subsurface properties. In Figure 4, the yellow triangles represent initial guesses (i.e. inversion

The Cryosphere Discuss., https://doi.org/10.5194/tc-2019-91
Manuscript under review for journal The Cryosphere
Discussion started: 15 May 2019




parameter combination starting points). In these plots, the synthetic truth is indicated by the intersection of the two dotted lines. Bright turquoise lines connecting yellow triangles with red dots represent the path that the LM algorithm has taken from the initial guess to the estimated parameter combination represented by the red dot. The dots connecting turquoise lines indicate the location at each LM iteration. Figure 4 indicates that the method is able to recover porosities more robustly than thermal conductivities. According to the liquid saturation plot on Figure 3, liquid saturation of the mineral layer is quite dynamic and more saturated in comparison to the peat layer. Nevertheless, thermal conductivity of the mineral layer corresponds to the highest uncertainty. Three out of thirty red dots corresponding to thermal conductivity of mineral soil end up close to 1.4 $W\ m^{-1}K^{-1}$ (the true value is 2 $W\ m^{-1}K^{-1}$), suggesting those values do not correspond to the 'truth', since most of the estimated values (27 cases) are concentrated around the intersection of the dotted lines. In this case the response surface for the corresponding cost function (eqn. 3) lies in a flat, low-gradient region. This effect can be seen in Figure 5, the cost function corresponding to the estimated porosities (Figure 5A) has only one minimum, where the cost function corresponding to thermal conductivities (Figure 5B) has an elongated flat minima region indicating non-uniqueness of the estimated parameters. This case corresponds to the 6 near-surface observation points (Figure 2A) with short vertical distance between the points. The close proximity of the observation locations might be limiting variability in the calibration targets leading to difficulty in estimating the $k_m$ parameter.

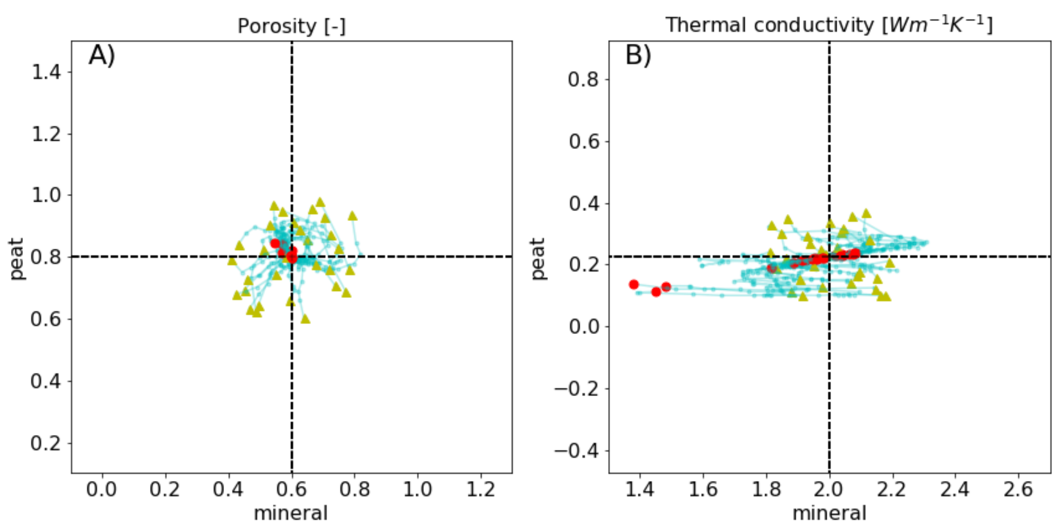

The Cryosphere Discuss., https://doi.org/10.5194/tc-2019-91
Manuscript under review for journal The Cryosphere
Discussion started: 15 May 2019


**Figure 4.** Estimated values of a sample of 30 initial guesses to their "true" values shown as a cross-section of two dotted lines for A) porosities and B) thermal conductivities for peat mineral soil layers. Blue lines correspond to different paths that have been taken by the LM algorithm. The red dots correspond to the estimated parameter values. Note that subfigures (A) and (B) are each showing 2D projections of the 4D parameter space of the inversion.

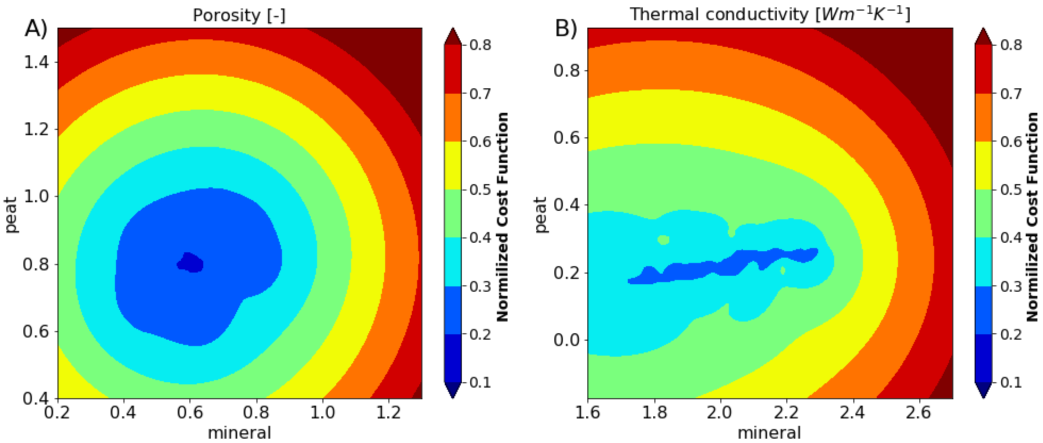


**Figure 5.** Cost function corresponding to A) porosities and B) thermal conductivities for peat and mineral soil layers. Here, the colorbar is a normalized cost function. Note that subfigures (A) and (B) are showing 2D projections of a 4D parameter space that the inverse approach was applied to.

Figure 6 illustrates estimated parameters for all cases corresponding to simplified meteorological data from Table 2. Figure 6AB shows good convergence of the (S)6$T6s_l1r$ case for porosities and worse convergence for thermal conductivities with an averaged error of 0.1$Wm^{-1}K^{-1}$. Adding noise to the (S)6$T6s_l1r$+$n$ case slightly worsens the estimated porosity values and significantly worsens mineral soil thermal conductivity with RMSE raising from 10% to more than 50% (Figure 6CD). Figure 6EF shows that increasing the number of the monthly ERT profiles from 1 to 8 improved soil property estimates, allowing four out of five PE runs to converge closer to the synthetic truth. If we do not consider the one outlier on the conductivity plot (Figure 6F) for case (S)6$T6s_l8r$+$n$ then uncertainty is smaller than for the (S)6$T6s_l1r$ case (without noise), suggesting that despite introduction of the 10% noise to the ERT data increasing the number of the monthly ERT profiles improves the overall PE.

The Cryosphere Discuss., https://doi.org/10.5194/tc-2019-91
Manuscript under review for journal The Cryosphere
Discussion started: 15 May 2019


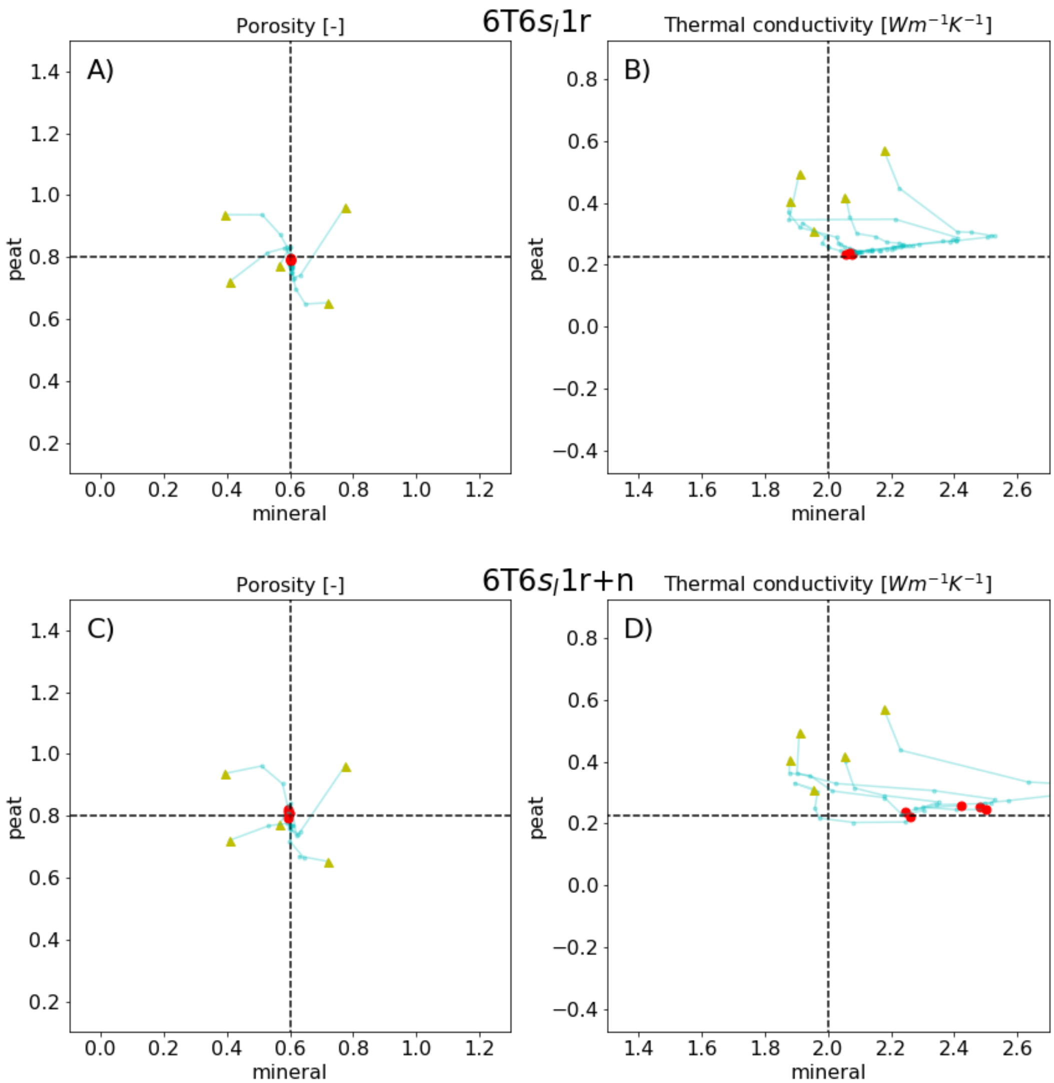

The Cryosphere Discuss., https://doi.org/10.5194/tc-2019-91
Manuscript under review for journal The Cryosphere
Discussion started: 15 May 2019


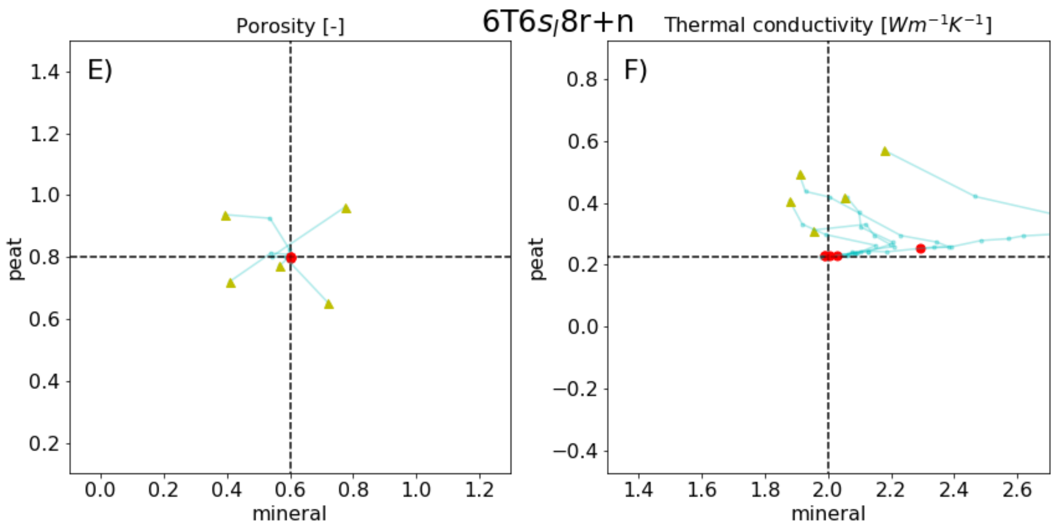


**Figure 6.** Estimated values of a sample of 5 initial guesses to their "true" values shown as a cross-section of two dotted lines for the bulk porosities and bulk thermal conductivities for peat mineral soil layers. Blue lines correspond to different paths that have been taken by the LM algorithm. The red dots correspond to the estimated values. A-B) 6 observation points and 1 ERT resistance profile (S)$6T6s_l1r$; C-D) 6 observation points and 1 ERT resistance profile with added noise (S)$6T6s_l1r{+}n$; E-F) 6 observation points and 8 ERT resistance profile with added noise (S)$6T6s_l8r{+}n$. Note that the plots are each 2D projections of the 4D parameter space of the inversion.

In Figure 7, we summarize results from the five PE runs for the first six cases corresponding to simplified meteorological data listed in Table 2. The first row of tables corresponds to the final root-mean-squared error (RMSE) values for each measurement type ($\Delta T$, $\Delta s_l$, and $\Delta r$). The second row of tables corresponds to the Euclidian distances between the synthetic truth and estimated parameter values of $\delta\phi$ and $\delta k$. As it was shown above, the method is able to accurately estimate both peat and mineral soil porosities and peat layer thermal conductivity ($k_p$), but cannot always accurately estimate the thermal conductivity of the mineral soil ($k_m$). That is why the matrix table with estimated thermal conductivities on Figure 7 shows the highest discrepancy (bottom row, last table). However, one can see from the $\phi$ and $k$ matrix tables that increasing the number of monthly ERT profiles improves the estimates of $\phi$ and $k$. This suggests that by increasing the number of monthly ERT profiles, we are improving the convexity of the cost function (eqn.3). Increasing the number of $T$ and $s_l$ observational points from 3 to 6 has a less significant effect on estimated values of $\phi$ and $k$. This could be due to the fact that all 6 observational points lie within the active layer zone. Suggesting that adding observations below the active layer might have more significant effect on the estimated properties. Therefore, we added extra observational points (red stars in Figure 2A), to test this assumption in the experiment with actual meteorological data.

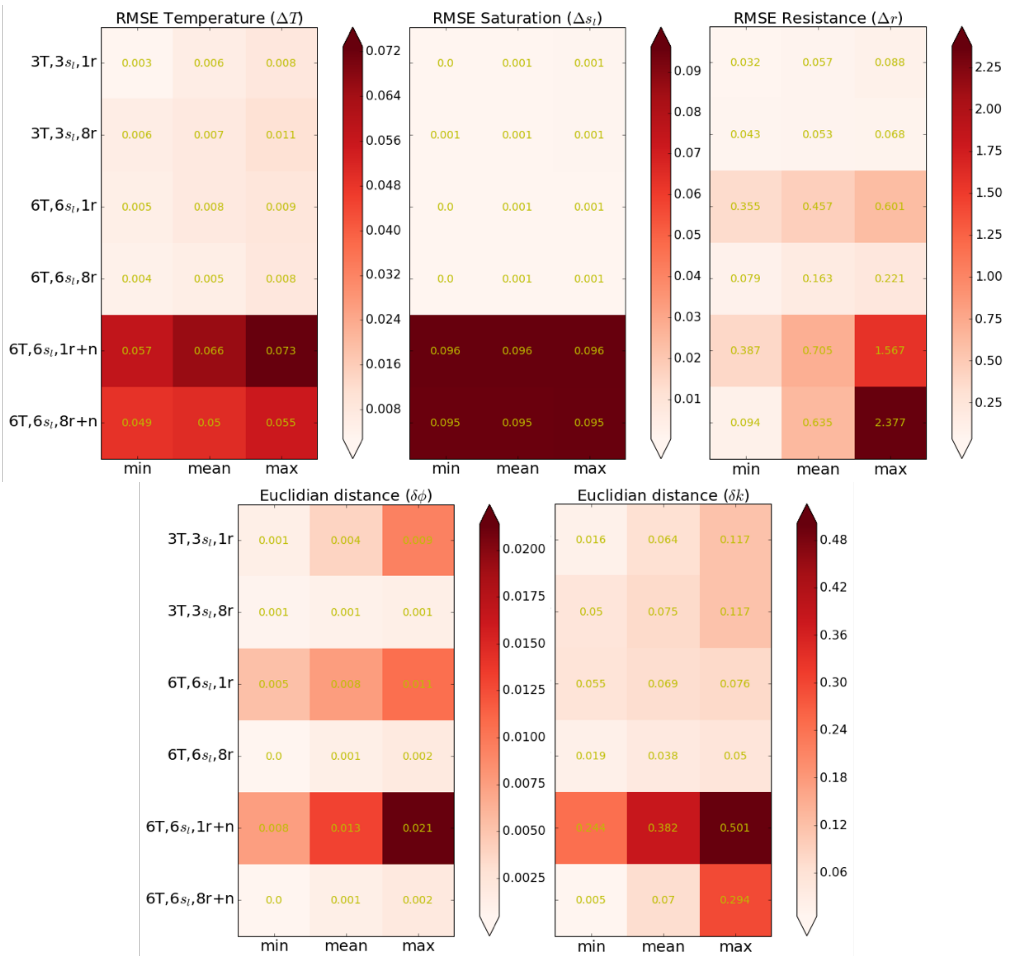


**Figure 7.** Five matrix tables presenting fitness metrics between synthetic model values and values obtained by the parameter estimation method using simplified meteorological data. First row corresponds to the root mean squared errors for temperatures, liquid water saturations, and resistances. Second row includes tables corresponding to Euclidian distances between synthetic ("true") and estimated parameter values.

**3.2 Meteorological data from Utqiagvik (Barrow) site 2015**

The Cryosphere Discuss., https://doi.org/10.5194/tc-2019-91
Manuscript under review for journal The Cryosphere
Discussion started: 15 May 2019


After testing the PE method for the simplified meteorological data, we applied measured meteorological data from the BEO site for year 2015. To better understand the importance of each measurement type and their combinations within the developed PE framework we tested all of the scenarios corresponding to the 'actual meteorological data' column from Table 2. The results of these runs are summarized in the colored matrix tables in Figure 8. Since there are twice the number of actual meteorological cases than the simplified meteorological cases, it is hard to analyze all matrix tables at once. To combine the data from all five matrices we normalized the mean values in the middle column in each table by their maximum value as $\widetilde{\Delta} = \frac{\Delta}{\Delta_{max}}$ and $\tilde{\delta} = \frac{\delta}{\delta_{max}}$. This normalized the magnitudes of different measurement and soil property types. Then we calculated the RMSE of the normalized mean values for combined measurement and soil property types, $\Delta(\widetilde{\Delta \mathrm{T}}, \widetilde{\Delta \mathrm{s_l}}, \widetilde{\Delta \mathrm{r}})$ and $\Delta(\widetilde{\delta\phi}, \widetilde{\delta \mathrm{k}})$, respectively . Based on these normalized and combined RMSE values, we used k-mean clustering analysis to identify groupings of data collection strategies that result in similarly performing inversions. The analysis identified four clusters of data collection strategies resulting in similarly performing inversions shown in Figure 9. Class I and II indicate all the cases that provide good accuracy for the estimated properties. Class I indicates the best cases that provide an accurate parameter estimation as well as accurate matches with the synthetic "true" measurements. Class II includes the cases that have accurate parameter estimates and less accurate matches with the measurements. Class III indicates all cases that have less accurate parameter estimates but accurate matches with the measurements. Finally, Class IV includes the cases that showed the worst performance in terms of parameter estimates and the worst matches with the measurements. We summarized the results from Figure 9 in Table 3.

Cases in Class I (see Table 3) suggest that measurement locations below the active layer lead to better PE, meaning that by increasing the number of measurement locations leads to more accurate parameter estimation. In contrast, the last element of the first class is a case with one ERT profile ($1r$), suggesting that one ERT profile could be enough for effective parameter estimation. This is due to the design of this numerical experiment, i.e. due to the fact that we are using a synthetic "truth" produced by the same model used in the inversion, which improves the convexity of the cost function and leads to a well constrained unique minimum. However, in reality, collection of the additional information, such as organic layer thickness and temperature data, are extremely important and are required for model calibration (Jafarov et al., 2012; Atchley et al., 2015). In addition, real ERT surveys can be perturbed by noise and their interpretation may require site-specific petrophysical relationships as opposed to the general petrophysical relationships used in this study. Therefore, we do not suggest to collect only one ERT measurement without any additional data.

Class II indicates that increasing the number of monthly ERT profiles is important for more accurate PE. However, increasing the number of ERT profiles leads to a less accurate match with measurements. These results are consistent with the previous results for simplified data and added noise (Figure 6).

Class III includes 6 cases suggesting that if we have only soil moisture data available for PE, then we should expect less accurate soil property estimates. The last element in this class suggests that collecting daily resistance profiles improves the resistance match (Figure 8, resistivity table) but does not improve soil property estimates, where monthly ERT profiles improve thermal conductivity convergence.

Class IV once again clearly indicates that measurements obtained below the active layer provide more accurate parameter estimates, however, they do not improve matches to measurements. This is mainly due to significant mismatch with the ERT data, which can be seen on the RMSE resistance table (Δr) in Figure 8. In reality, the depth of the mineral soil can be deeper than 20 cm, not having sensors lower than 20 cm limits the amount of data that can help to improve the convexity of the cost function in our case.

**Table 3:** K-mean analysis of the accuracy for each 13 cases.

| Class I | Class II | Class III | Class IV |
|---|---|---|---|
| $10T\,10s_l1r$ | $6T\,6s_l8r$ | $6s_l$ | $10T$ |
| $10T\,10s_l8r$ | $3T\,3s_l8r$ | $6s_l1r$ | $6T$ |
| $1r$ | | $6T\,1r$ | |
| | | $3T\,3s_l1r$ | |
| | | $6T\,6s_l$ | |
| | | $6T\,6s_l8r(s)$ | |

From Figure 9 and Table 3 we know that the *6T* case has the worst performance in terms of matching $\{\phi, k\}$. Similar to the experiments with simplified meteorological data, the main difficulty for experiments with actual meteorological data is matching thermal conductivity. The

The Cryosphere Discuss., https://doi.org/10.5194/tc-2019-91
Manuscript under review for journal The Cryosphere
Discussion started: 15 May 2019




last matrix table ($\sigma(k)$) on Figure 9 shows that $6T6s_l8r(s)$ has the highest maximum and mean mismatch in thermal conductivity estimates. However, since $\phi$ estimates are a better match with their corresponding "true" values, the case $6T6s_l8r(s)$ falls into class III in Figure 9, as opposed to case $6T$, which falls into class IV. The highest mismatch in thermal conductivity values for the $6T6s_l8r(s)$ case suggests that collecting daily resistance profiles improves the resistance match (Figure 8, resistivity table) but does not improve estimated parameters, where monthly ERT profiles improve thermal conductivity estimation.

To illustrate this, we plot values of estimated thermal conductivities and the corresponding cost functions for cases $10T10s_l8r$ and $6T6s_l8r(s)$ on Figure 10. The PE method was able to match 4 out of 5 points perfectly and missed the $k_p$ for the $10T10s_l8r$ case. The corresponding cost function is almost perfectly convex with only one minimum. In contrast to this, the $6T6s_l8r(s)$ case completely missed 2 points by converging on values outside the boundaries, and 3 other points do not converge to the desired cross section as well. The corresponding cost functions does not have a well-defined global minimum.

## 4. Discussion

The existence of multiple minima is common in inverse modeling and leads to false convergence of the LM algorithm and physically non-realistic subsurface parameters (Nicolsky et al., 2007). This is one of the main reasons of using multiple initial guesses. We suggest to run at least ten different initial guesses. If most of those runs converge to a similar set of values with the lowest cost function value, then that set of values is most likely the global minimum.

There will always be cases like $6T6s_l8r(s)$, where all runs converge to different values of $k_m$, indicating that using certain combinations of datasets does not allow the inverse approach to properly recover $k_m$. It is likely that $6T6s_l8r(s)$ does not capture much variability in soil temperatures and soil moisture and therefore ERT profiles do not have much variability as well. Once the cost function converges for one of the ERT profiles, it immediately converges on the other daily profiles. In fact, although $6T6s_l8r(s)$ has a good accuracy with observations (see the "RMSE Resistance" table in Figure 8), it is unable to recover the value of $k_m$. Here, a regularization technique may improve the corresponding data accuracy. The regularization

The Cryosphere Discuss., https://doi.org/10.5194/tc-2019-91
Manuscript under review for journal The Cryosphere
Discussion started: 15 May 2019


techniques have been widely used in solving ill-posed inverse problems (Vogel, 2002). Its overall idea is to constrain the objective function by imposing additional priors on the estimated model parameters. The PEST package allows us to add a regularization term to the cost function (eqn. 4). In particular, the PEST package provides several categories of regularization techniques including Tikhonov regularization, subspace-type of regularization, and hybrid regularization. Tikhonov regularization, being the most commonly used regularization technique in inverse problems, imposes a $L_2$ norm constraint on the estimated model parameters (Vogel, 2002). The resulting cost function tends to be smoother over the parameter space. The subspace regularization technique is developed based on truncated singular value decomposition. It promotes the numerical stability of the iteration by discarding the eigenvectors associated with small singular values so that the solution space can be spanned by the dominant eigenvectors. The hybrid regularization technique is a combination of Tikhonov regularization and subspace regularization techniques. The numerical results presented in this manuscript demonstrates that our problems may not be severely ill-posed. Hence, reasonable results can be obtained with enough data coverage. Having regularization techniques incorporated into our current method may help to constrain the estimated parameters from significant divergence as in Figure 10C. However, exploration of the regularization options in PEST requires in depth experimentation beyond the scope of the current study.

We have shown that even in the ideal situation where we either generate observational data or use simplified meteorological data, we cannot always fit modeling results to observations. In reality, noise (e.g. sensor's measuring resolution) contaminates the observational data. To investigate the impact of measurement noise, we introduced multiple levels of noise to the simplified meteorological data. The PE showed that dealing with noisy data is challenging, even for a simple cases (Figure 6). However, our analysis showed that adding more data into the cost function (in particular resistivity data) can improve the overall PE accuracy.

The distance between sensors could be another reason that might lead to the uncertainty in PE. As it was pointed out by Nicolsky et al., (2009), it is important to make sure that a vertical difference between the adjacent measurements do not introduce additional noise that can confuse the minimization algorithm. If sensors are really close to each other, then measurements might be the same or within the noise variability. In our setup the vertical distance between the first 6 sensors is about 10cm. This could lead to small temperature variability between sensors. Indeed, providing greater vertical distance between observational points improved the PE accuracy (see cases with 10 observational points).

Combining hydrothermal observations from multiple depths with monthly ERT measurements resulted in improving the shape of the cost function leading to better defined minima (Figure 10). Increasing the number of the monthly ERT profiles improved the accuracy of the estimated data. In addition, we showed that having observation points below the ALT combined with ERT profiles shows the best accuracies both in the terms of estimating parameters and matching observations.

## 5. Conclusion

The overarching goal of this study was to validate a newly developed PE framework using a synthetic setup and 2D coupled thermal-hydro-geophysical model based on the polygonal tundra at the BEO study site. The results of this study show that estimating subsurface properties even for a synthetic setup can be quite complicated. Nevertheless, the PE method evaluated here shows that there are cases when the method is able to robustly recover synthetic properties. The robustness of the method depends on the frequency and diversity of the collected data. For example, we found that adding monthly ERT surveys into the cost function significantly improves the accuracy of the estimated properties. It is important to note that to improve the overall robustness of the PE, it is better to collect such data from multiple depths within and below the active layer. Furthermore, we conclude that different data types query the system in different ways; we find that the most robust predictions result from inversions that include multiple data types.

As it was shown in this study, different measurement types as well as a combination of multiple measurements might lead to the different shapes of the cost function with multiple minima and/or ill-defined global minimum (flat spots in the response surface). To improve the overall PE performance we suggest the following: 1) restricting of the parameter range to better constrain the local minimum; 2) introducing different types of data ($T, s_l, r$) into the cost function to improve PE accuracy. If most of the runs from the sample converge to the same parameter values and the cost function is lower at this location, then those values most likely correspond to the actual soil properties. The ability to refine the cost function with more data (monthly ERT and timeseries from multiple depths) has to be further explored with actual data.

The Cryosphere Discuss., https://doi.org/10.5194/tc-2019-91
Manuscript under review for journal The Cryosphere
Discussion started: 15 May 2019


The Cryosphere
Discussions
Open Access

Implication of the PE method to the actual measured data might require adjustment of the initial conditions of the model (saturation and temperature). Incorporating the initial condition data into the PE framework might lead to a better match with actual subsurface observations. This work demonstrates the feasibility of the developed PE framework. However, further evaluation of regularization methods and recovery of the soil properties using measured subsurface data from the BEO site is needed and are beyond the scope of the current paper.

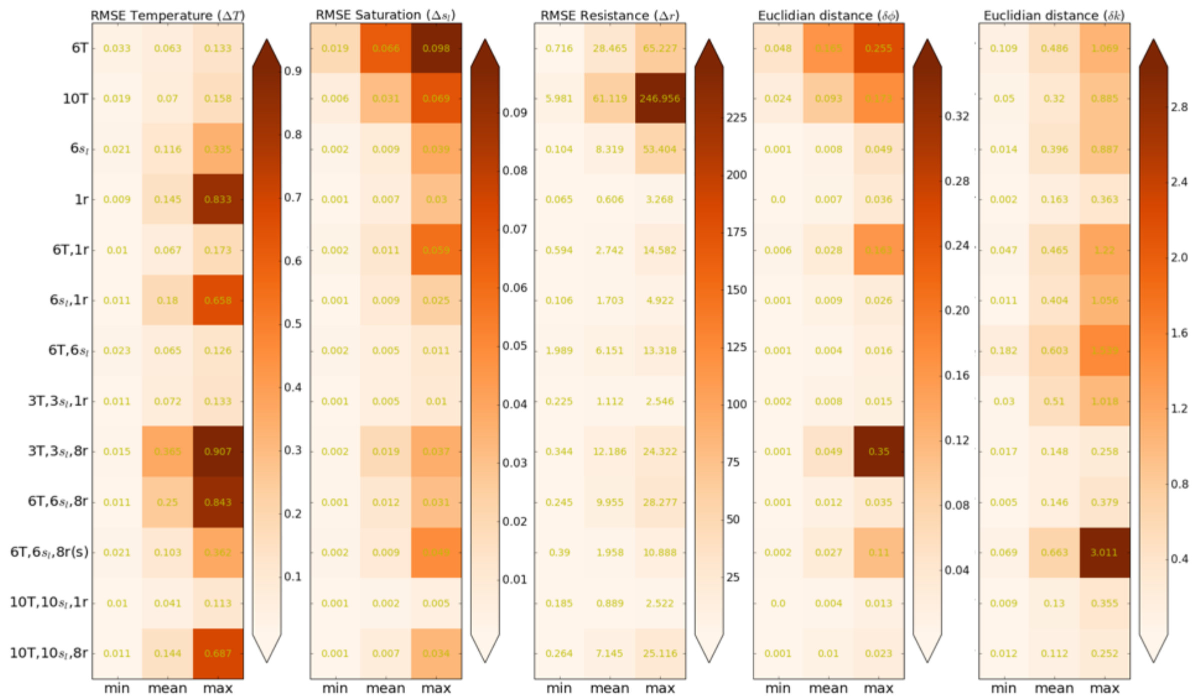


**Figure 8.** Five matrix tables represent fitness metric between synthetic model values and values obtained by the parameters estimation method using meteorological data from year 2015 from BEO site in Alaska. First three tables correspond to the root mean squared values for temperatures, liquid water saturations, and resistances, the last two tables correspond to Euclidian distances between synthetic and estimated conductivities and porosities, correspondingly.

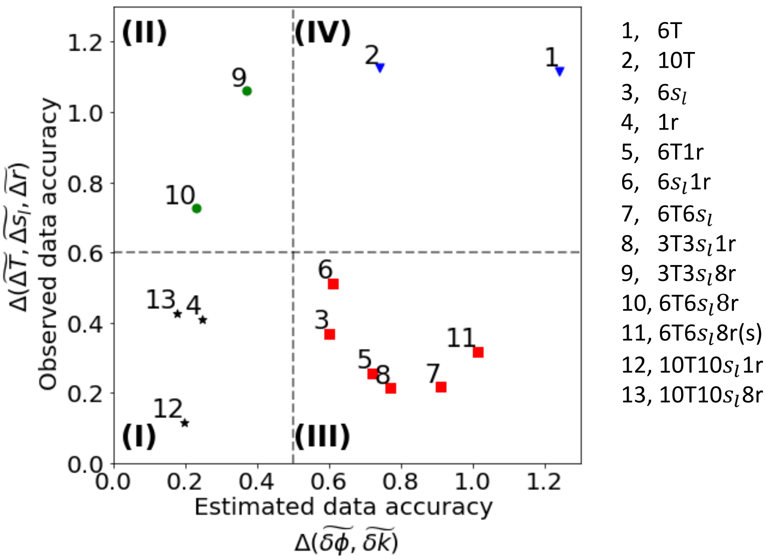


**Figure 9.** A k-mean analysis applied to the RMSE of the normalized means of estimated soil properties and the corresponding fit between calculated and observed values. Each color and marker represent a certain class as result of the k-mean cluster analysis.

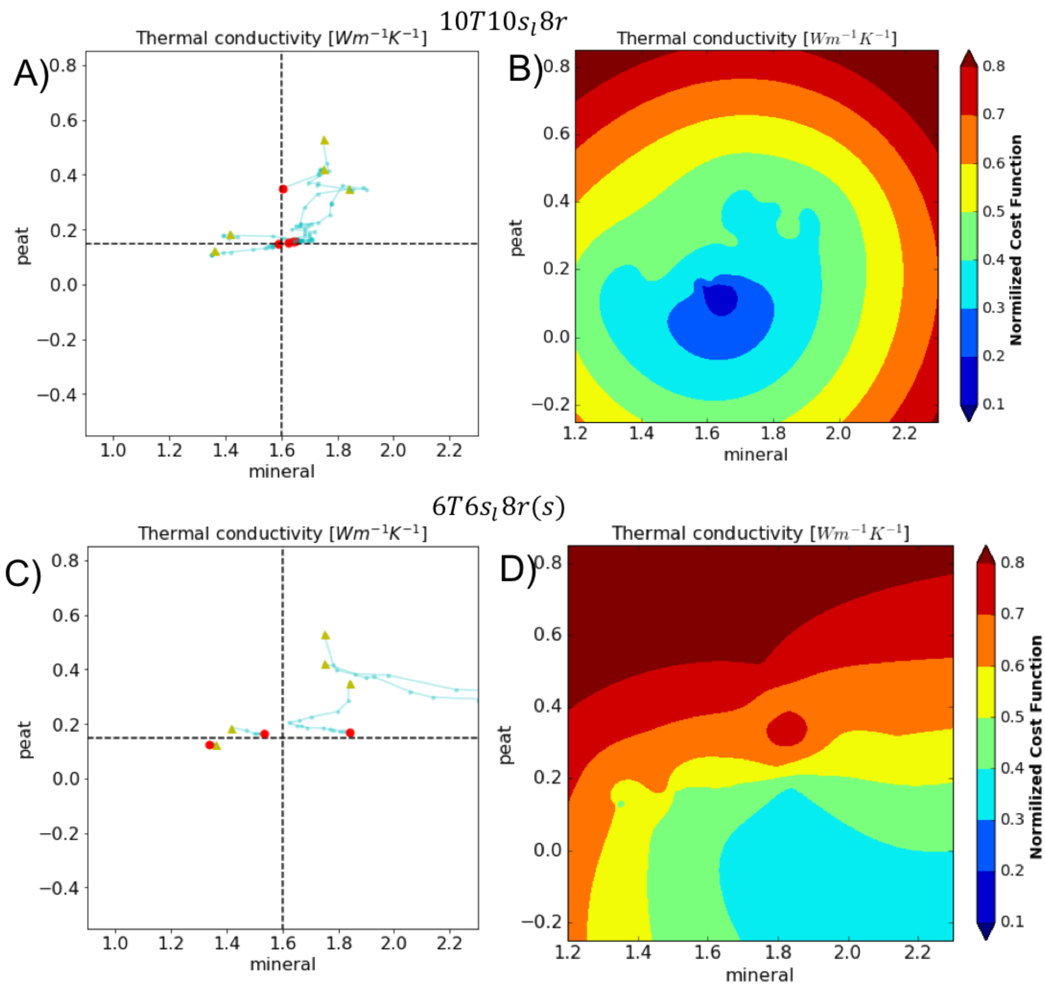


**Figure 10**. A) and C) parameter search trajectories for 5 inversions where the "true" values are shown as a cross-section of two dotted lines for the bulk porosities and bulk thermal conductivities for peat mineral soil layers. Blue lines correspond to different paths that have been taken by the LM algorithm. The red dots correspond to the estimated parameter values. First row corresponds to 10 measurement locations and 8 ERT resistance monthly profiles ($10T10s_l8r$), and the second row corresponds to 6 measurement locations and 8 ERT resistance daily profiles ($6T6s_l8r(s)$). B) and D) the colormap plots on the right represent the cost function values associated with the corresponding thermal conductivities.

## 5. Acknowledgements

This work is part of the Next-Generation Ecosystem Experiments (NGEE Arctic) project which is supported by the Office of Biological and Environmental Research in the DOE Office of Science.

## 6. References

Abolt, C. J., Young, M. H., Atchley, A. L., and Harp, D. R.: Microtopographic control on the ground thermal regime in ice wedge polygons, The Cryosphere, 12, 1957-1968, https://doi.org/10.5194/tc-12-1957-2018, 2018.

Alifanov, O., Artyukhin, E., Rumyantsev, S., 1996. Extreme Methods for Solving Ill-posed Problems with Application to Inverse Heat Transfer Problems. Begell House, New York.

Atchley, A. L., Painter, S. L., Harp, D. R., Coon, E. T., Wilson, C. J., Liljedahl, A. K., and Romanovsky V.E.. 2015 Using field observations to inform thermal hydrology models of permafrost dynamics with ATS (v0.83) Geosci. Model Dev. 8 2701–22

Beck, J., Clair, C.S., Blackwell, B., 1985. Inverse Heat Conduction: Ill-Posed Problems. Wiley, New York.

Biskaborn et al., Permafrost is warming at a global scale, Nature Communications. 2019. Volume 10, Number1, Pages 264, doi 10.1038/s41467-018-08240-4.

Boike, J. and Roth, K.: Time domain reflectometry as a field method for measuring water content and soil water electrical conductivity at a continuous permafrost site, Permafrost Periglac., 8, 359–370, 1997.

Dafflon, B., Oktem, R., Peterson, J., Ulrich, C., Tran, A. P., Romanovsky, V., and Hubbard, S.: Coincident above and below-ground autonomous monitoring strategy: Development and use to monitor Arctic ecosystem freeze thaw dynamics, J. Geophys. Res.-Biogeo., 122, 1321–1342, https://doi.org/10.1002/2016JG003724, 2017.

Doherty, J., 2001. PEST-ASP user's manual. *Watermark Numerical Computing, Brisbane, Australia*.

Harp, D. R., Atchley, A. L., Painter, S. L., Coon, E. T., Wilson, C. J., Romanovsky, V. E., and Rowland, J. C.: Effect of soil property uncertainties on permafrost thaw projections: a calibration-constrained analysis, The Cryosphere, 10, 341-358, https://doi.org/10.5194/tc-10-341-2016, 2016.

The Cryosphere Discuss., https://doi.org/10.5194/tc-2019-91
Manuscript under review for journal The Cryosphere
Discussion started: 15 May 2019


Hjort, J., Karjalainen, O., Aalto, J., Westermann, S., Romanovsky, V. E., Nelson, F. E. Etzelmüller, B., and Luoto, M. Degrading permafrost puts Arctic infrastructure at risk by mid-century. Nature Communications. 2018. Volume 9, Number1, Pages 5147, doi 10.1038/s41467-018-07557-4.

Jafarov, E. E., Marchenko, S. S., and Romanovsky, V. E.: Numerical modeling of permafrost dynamics in Alaska using a high spatial resolution dataset, The Cryosphere, 6, 613-624, doi:10.5194/tc-6-613-2012, 2012

Jafarov, E.E., Coon E. T., Harp, D.R., Wilson, C. J., Painter, S. L., Atchley, A.L., Romanovsky V.E.: (2018) Modeling the role of preferential snow accumulation in through talik development and hillslope groundwater flow in a transitional permafrost landscape. Environ. Res. Lett, 2018. https://doi.org/10.1088/1748-9326/aadd30.

Johansen, O. 1977. Thermal Conductivity of Soils No. CRREL-TL-637 Cold Regions Research and Engineering Lab, Hanover NH

Kern, J. S.: Spatial Patterns of Soil Organic Carbon in the Contiguous United States, Soil Sci. Soc. Am. J., 58, 439–455, 1994.

Koven, C. D., Riley, W. J., and Stern, A.: Analysis of permafrost thermal dynamics and response to climate change in the CMIP5 earth system models, J. Climate, 26, 1877–1900, doi:10.1175/JCLI-D-12–00228.1, 2013.

Levenberg, K.. A method for the solution of certain non-linear problems in least squares, Quart. Appl. Math., 2 (1944), pp. 164–168. [28]

Marquardt, D. W.. An algorithm for least-squares estimation of nonlinear parameters, J. Soc. Ind. Appl. Math., 11 (1963), pp. 431–441.

McKay, M.D.; Beckman, R.J.; Conover, W.J. 1979. A Comparison of Three Methods for Selecting Values of Input Variables in the Analysis of Output from a Computer Code. American Statistical Association. 21 (2): 239–245. doi:10.2307/1268522

McGuire A D et al 2018. The dependence of the evolution of carbon dynamics in the northern permafrost region on the trajectory of climate change Proc. Natl Acad. Sci. 115, 3882–7

Nicolsky, D. J., Romanovsky, V. E., and Tipenko, G. S.: Using in-situ temperature measurements to estimate saturated soil thermal properties by solving a sequence of optimization problems, The Cryosphere, 1, 41-58, https://doi.org/10.5194/tc-1-41-2007, 2007.

Nicolsky, D.J., Romanovsky, V.E., Panteleev, G.G., 2009. Estimation of soil thermal properties using in-situ temperature measurements in the active layer and permafrost. Cold Reg. Sci. Technol. 55 (1), 120–129.

Painter S L, Coon E T, Atchley A L, Berndt M, Garimella R, Moulton JD, Svyatskiy D., and Wilson, C., J.. 2016 Integrated surface/subsurface permafrost thermal hydrology: model formulation and proof-of-concept simulations Water Resour. Res. 52 6062–77

Peters-Lidard, C. D., Blackburn, E., Liang, X., and Wood, E., F. 1998 The effect of thermal conductivity parameterization on surface energy fluxes and temperatures J. Atmos. 55 1209–24

Romanovsky, V. E. *et al.* [The Arctic] Terrestrial Permafrost. In: State of the Climate in 2015. S149-S152 (2015).

Rücker, C., Günther, T., and Spitzer, K.: Three-dimensional modelling and inversion of DC resistivity data incorporating topography – I. modelling, Geophys. J. Int., 166, 495–505, https://doi.org/10.1111/j.1365-246X.2006.03010.x, 2006

Schuster, P. F., K. M. Schaefer, G. R. Aiken, R. C. Antweiler, J. F. DeWild, J. D. Gryziec, A. Gusmeroli, G. Hugelius, E. Jafarov, D. P. Krabbenhoft ,L. Liu , N. Herman-Mercer, C. Mu, D. A. Roth, T. Schaefer, R. G. Striegl, K. P. Wickland, and T. Zhang (2018), Permafrost stores globally significant amount of mercury, Geophys. Res. Lett, 45, GRL56886, DOI: 10.1002/2017GL075571

Smith, M. and Tice, A.: Measurement of the unfrozen water content of soils comparison of NMR and TDR methods, CRREL Report 88-18, US Army Cold Regions Research and Engineering Lab, 16 pp., 1988.

Tran, A. P., Dafflon, B., and Hubbard, S. S.: Coupled land surface–subsurface hydrogeophysical inverse modeling to estimate soil organic carbon content and explore associated hydrological and thermal dynamics in the Arctic tundra, The Cryosphere, 11, 2089-2109, https://doi.org/10.5194/tc-11-2089-2017, 2017.

Oleson, K. W., Lawrence, D. M., Gordon, B., Bonan, G. B., Drewniak, B., Huang, M., Koven, C. D., Levis, S., Li, F., Riley, J. W., Subin, Z. M., Swenson, S. C., and Thornton, P. E.: Technical description of version 4.5 of the Community Land Model (CLM), NCAR Technical Note NCAR/TN-503CSTR, 420 pp., https://doi.org/10.5065/D6RR1W7M, 2013.

The Cryosphere Discuss., https://doi.org/10.5194/tc-2019-91
Manuscript under review for journal The Cryosphere
Discussion started: 15 May 2019


Vogel, C.R.. Computational Methods for Inverse Problems. 2002. 183 pages. SIAM. ISBN: 9780898715507

Yoshikawa, K., Overduin, P., and Harden, J.: Moisture content measurements of moss (Sphagnum spp.) using commercial sensors, Permafrost Periglac., 15, 309–318, 2004.

Wang, K., Jafarov, E., Overeem, I., Romanovsky, V., Schaefer, K., Clow, G., Urban, F., Cable, W., Piper, M., Schwalm, C., Zhang, T., Kholodov, A., Sousanes, P., Loso, M., and Hill, K.: A synthesis dataset of permafrost-affected soil thermal conditions for Alaska, USA, Earth Syst. Sci. Data, 10, 2311-2328, https://doi.org/10.5194/essd-10-2311-2018, 2018.